
Rideal Lecture

Universal features of the fluid to solid transition for attractive colloidal particles

V. Prasad,^a V. Trappe,^b A. D. Dinsmore,^c P. N. Segre,^d L. Cipelletti^e and D. A. Weitz^a

^a Department of Physics and DEAS, Harvard University, Cambridge MA 02138, USA

^b Department of Physics, University of Fribourg, CH-1700, Fribourg, Switzerland

^c Department of Physics, University of Massachusetts, Amherst MA 01003, USA

^d Bio-Physics Group, NASA Marshall Space Flight Center, Huntsville AL 35812, USA

^e Department of Physics, University of Montpellier II, F-34095, Montpellier, France

Received 11th November 2002, Accepted 11th November 2002

First published as an Advance Article on the web 22nd November 2002

Attractive colloidal particles can exhibit a fluid to solid phase transition if the magnitude of the attractive interaction is sufficiently large, if the volume fraction is sufficiently high, and if the applied stress is sufficiently small. The nature of this fluid to solid transition is similar for many different colloid systems, and for many different forms of interaction. The jamming phase transition captures the common features of these fluid to solid transitions, by unifying the behavior as a function of the particle volume fraction, the energy of interparticle attractions, and the applied stress. This paper describes the applicability of the jamming state diagram, and highlights those regions where the fluid to solid transition is still poorly understood. It also presents new data for gelation of colloidal particles with an attractive depletion interaction, providing more insight into the origin of the fluid to solid transition.

Introduction

The rheological properties of colloidal suspensions can vary enormously; they can range from low viscosity fluids to highly elastic pastes. The control of their properties is essential for any technological application, and represents one of the most interesting and important challenges in our understanding of colloidal suspensions. Their rheological properties are controlled to a large extent by the size and concentration of the particles and by the interactions among them. Because colloidal particles are intrinsically metastable, a strong repulsive interaction is essential to maintain stability. However, many technologically important colloidal suspensions can also have some form of attractive interaction between the particles, and this can have a dramatic effect on the rheological behavior of the suspension. The suspension properties depend critically on both the magnitude of the attractive energy between particles, U , as well as the volume fraction of particles, ϕ . Varying these can transform a colloidal suspension from a purely viscous fluid to a highly elastic solid.

There are two limiting cases of the fluid to solid transition which are well understood: The first is for very low volume fraction and very strong attractive interaction; the particles undergo diffusion-limited cluster aggregation (DLCA), forming fractal clusters which ultimately form a continuous, but tenuous network that spans the whole system, thereby becoming a solid that can bear stress.¹⁻⁴ Because the density of a fractal cluster decreases as it grows in size, DLCA will result in gelation at any volume fraction, however low. The second limiting case is for high volume fractions and no attractive interactions; the colloidal particles behave as hard spheres, and crowding can lead to a colloidal glass at $\phi_g \approx 0.58$, where the particles become caged and can no longer diffuse freely.⁵ In this case the suspension again behaves as an elastic solid, where the elasticity is due to the resistance to distortion of the average particle configurations, and is entropic in nature.^{6,7} At even higher ϕ , the particles touch each other to achieve the highest possible packing of random uniform spheres, random close packing, with $\phi_{rcp} \approx 0.63$. Between these two limiting cases, there is a wide range of fluid to solid transitions which occur at intermediate values of U and ϕ ; colloidal gelation in this regime has been widely studied, yet the behavior of the transition, and the onset and nature of the stress-bearing properties of the solid-like phase, remain poorly understood.

Despite our incomplete understanding, all the fluid to solid transitions in colloidal suspensions have many features in common. In all cases, the fluid to solid transition involves crowding of aggregates, leading to an arrest of their kinetics. In all cases, there is a well defined value of the volume fraction for the transition, ϕ_c , which depends on the strength of the interparticle attraction. In all cases, a critical feature of the solid is that it can bear stress, and that it can be transformed back into a fluid when a sufficiently large shear stress, σ , is imposed. In an attempt to capture the commonality of all of these fluid to solid transitions, we suggested the possibility of using the jamming transition to characterize the behavior of attractive colloidal particles.⁸ This is an extension of a concept first introduced by Liu and Nagel⁹ to describe the behavior of repulsive systems, ranging from molecular glasses to granular systems. They suggested that these systems could be described by means of a phase or state diagram in three dimensions, with the inverse of the density, the temperature and the applied load as the axes. Increases in any of these parameters would transform a solid into a fluid. They also suggested that the jamming concept could be further generalized and be applied to attractive particles; in this case, the attractive interaction would replace the role of the osmotic pressure or confining stress which sets the density of repulsive particles. The application of the jamming concept to attractive colloidal particles allows the wide variety of fluid to solid transitions to be described within a single framework.

In applying the jamming concept to attractive particles, the density is replaced by the particle volume fraction, and it is the particles themselves that undergo the jamming transition from fluid to solid; the solvent is a background fluid. Moreover, the temperature of the system must be normalized by the magnitude of the attractive interaction, which is the control parameter for colloidal systems. Thus, the density axis is replaced by ϕ^{-1} and the temperature axis is replaced by $k_B T/U$, while the third axis remains the stress, σ . An underlying assumption of the jamming picture is the concept that ϕ , U and σ each play similar roles in controlling the arrest of kinetics. The jammed or solid region is near the origin, and the phase boundary to the fluid state exists as a surface in the three dimensional state diagram. A fluid to solid, or jamming transition occurs if ϕ^{-1} decreases, if U^{-1} decreases, or if σ decreases; in this sense, each parameter can be viewed as playing the role of an effective temperature that governs the kinetics of the particles of the suspension. The jamming transition focuses on the stress-bearing features of the solid, thereby providing important insight about the nature of solid. The phase boundary in the σ -plane represents the critical value of the shear stress that a material can withstand before beginning to flow; this is a direct reflection of the elastic properties of the jammed state. The main utility of the jamming concept is that it allows all of the different regimes of the fluid to solid transition in attractive colloidal particles to be described within a single framework.

The goal of this paper is to reassess the status of jamming as applied to attractive colloidal particles, to clearly delineate the regimes of behavior that are understood and to identify the key issues that remain to be resolved. We briefly review the scaling behavior observed in the viscoelastic response of colloidal gels that highlights the existence of a fluid to solid transition and allows us to clearly identify the critical volume fraction where it occurs. We then present new data that explores the details of the transition in the absence of applied stress, and which highlights the

issues that are still poorly understood. We conclude with a review of the use of the jamming state diagram to describe the phase behavior of attractive colloidal particles, and the fluid to solid transition.

Scaling of viscoelasticity of colloidal gels

An essential criterion in establishing a fluid to solid transition in a colloidal suspension is an accurate method to determine the critical volume fraction, ϕ_c , or critical interaction potential, U_c , of the transition. Rheological measurements are the most direct measure of the state of the system, as they specifically probe the mechanical properties of the colloidal network. The determination of the phase boundary, by means of well defined values of ϕ_c or U_c , rests on our ability to measure the onset of an elastic modulus; this can be quite difficult if the modulus is very low, as is the case for the very tenuous solid networks which are formed at low ϕ and high U . For such systems, the measurement of the elasticity, and the identification of the onset of a solid network, is made feasible by a scaling behavior that is observed for the rheological data of attractive colloidal suspensions at larger U , once they cross the fluid to solid transition to form a solid network that spans the system.

This scaling of the viscoelastic response of attractive colloidal suspensions was first observed in a study of the rheology of carbon black.¹⁰ We use a suspension of carbon black in a mineral oil, and measure the frequency dependent linear viscoelastic moduli for several different concentrations of carbon black. We control the interaction between the particles by varying the concentration of dispersant which adsorbs on the surface of the carbon black, much like a surfactant, reducing the attractive interaction between the particles by sterically stabilizing them; thus by increasing the dispersant concentration we can decrease the magnitude of the attractive interaction. We measure the frequency dependent linear viscoelastic response, the storage modulus, $G'(\omega)$, and the loss modulus, $G''(\omega)$, for a series of samples with fixed U and varying volume fraction, and with fixed volume fraction and varying dispersant concentration. Provided ϕ is sufficiently high and the dispersant concentration is sufficiently low, all the data for both $G'(\omega)$ and $G''(\omega)$ can be scaled onto a single master curve. By contrast, data for very low ϕ or high dispersant concentration exhibit the hallmarks of a fluid, and can not be scaled onto the master curve.

An example of the master curve for carbon black is shown in Fig. 1(a). It consists of data with both ϕ and U varied, with each data set scaled by a factor a in frequency axis and a factor b in the modulus axis. The full master curve has been scaled to ensure that the cross over, where $G'(\omega_c) = G''(\omega_c)$, occurs at a scaled frequency of $\omega_c a = 1$, and that the low frequency plateau modulus, G'_p , corresponds to a scaled modulus of $G'(\omega)b = 1$. Because of the wide variation of

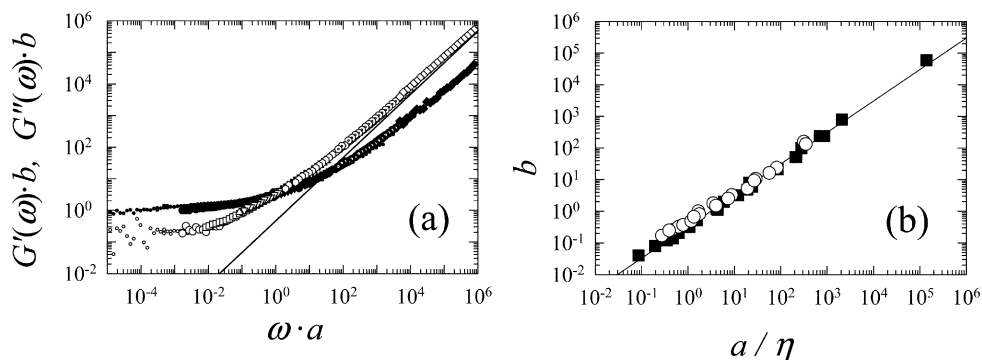


Fig. 1 (a) Master-curve showing the scaled moduli, $G'(\omega)b$ [solid symbols] and $G''(\omega)b$ [open symbols], as a function of scaled frequencies for carbon-black in mineral oil. Variation of ϕ at fixed interaction potential: [O] $\phi = 0.149$; [□] $\phi = 0.111$; [△] $\phi = 0.097$; [▽] $\phi = 0.078$; [⊗] $\phi = 0.073$; [○] $\phi = 0.064$; [◇] $\phi = 0.056$. Variation of U at fixed $\phi = 0.14$, small underlying circles. The solid line represents the viscosity of the background fluid. (b) Scale factors a and b for the different carbon-black [■] and PMMA/PS [○] systems; when b is plotted as a function of a/η , all scale factors fall onto a single curve, which increases linearly, as shown by the solid line.

samples used, the data extend over eleven decades of scaled frequency and seven decades of scaled modulus. The overall shape of the master curve is similar to that observed for many different soft materials.^{11–13} At low frequencies, $G'(\omega)$ dominates and is about an order of magnitude larger than $G''(\omega)$; moreover, $G'(\omega)$ is nearly frequency independent, while $G''(\omega)$ exhibits a weak minimum before starting to rise again at the very lowest frequencies. The frequency independent range of $G'(\omega)$ allows us to define a low frequency plateau in the elastic modulus, G'_p , which reflects the elasticity of the solid network. Above the crossover frequency, $G''(\omega)$ is greater than $G'(\omega)$, and asymptotically approaches a linear dependence with a value consistent with the viscosity of the background fluid, which is shown by the solid line in Fig. 1(a).

The origin of the scaling behavior can be described with a simple physical picture:¹⁰ The colloidal particles form a solid network which is interspersed with the background fluid; both the solid network and the fluid contribute independently to the measured moduli. The solid network of particles is elastic in nature, and has a frequency independent elastic modulus, whose magnitude depends sensitively on both ϕ and U . The background fluid is purely viscous in character, and thus contributes only to the loss modulus; therefore $G''(\omega)$ increases linearly with frequency and is independent of ϕ and U . The total response is the sum of the two independent contributions, with the contribution of the background fluid remaining roughly independent of the network, with the elastic contribution varying significantly with the strength of the network. The actual shape measured for any data set depends on the frequency range accessible in a rheometer. Then, any data set can be scaled onto the master curve by scaling both the frequency and the moduli by factors a and b , reflecting a scaling along the viscosity of the background fluid. A consequence of this simple picture is that the scaling factors for the modulus and the frequency must be linearly related. We test this hypothesis by plotting a , normalized by the viscosity of the solvent, as a function of b for all the data sets. As shown in Fig. 1(b), a linear relationship is observed, confirming the validity of the model for the scaling behavior.

An important consequence of this scaling is that the plateau modulus, G'_p , can be obtained for all samples from the factor, b , required to scale the data onto the master curve. This allows us to determine G'_p even for very weak networks, where the value of the plateau modulus is too low to be measured directly. We find that the plateau modulus grows in a critical fashion, with $G'_p = G_0(\phi - \phi_c)^{\nu_\phi}$, where for carbon black $\nu_\phi \approx 4.1$ and $\phi_c \approx 0.053$. This allows us to identify the presence of a critical value of the volume fraction for the fluid to solid transition and to accurately determine its value. The dependence of G'_p on U exhibits a similar critical behavior, allowing us to identify the critical value of the interaction energy, U_c , where the fluid to solid transition occurs. However, while there is clearly a critical value for both the volume fraction and interaction energy, it is difficult to determine the relationship between ϕ_c and U_c using the carbon black data because of uncertainty determining the relationship between U and the dispersant concentration.

Depletion gels

To investigate the relationship of ϕ_c and U_c , we use a model colloid system with an attractive interparticle interaction induced through the addition of polymer, leading to a depletion attraction.¹⁴ We use polymethyl-methacrylate (PMMA) spheres, stabilized by thin layers of poly-12 hydroxystearic acid, suspended in a mixture of cycloheptylbromide (CHB) and decalin that matches both the index of refraction and the density of the particles. These PMMA colloids are an excellent model system that has been widely investigated, and has been shown to behave as a nearly ideal hard sphere suspension, where the particles interact solely by volume exclusion.¹⁵ A depletion attraction is induced by the addition of polystyrene (PS); we use two molecular weights, $M_w = 2 \times 10^6 \text{ g mol}^{-1}$ and $M_w = 9.6 \times 10^4 \text{ g mol}^{-1}$. By varying the polymer concentration, we are able to vary the magnitude of the attractive interaction, which we calculate using the theory for the depletion interaction.¹⁶ By varying the molecular weight and thus the size of the depleting agent, we are able to vary the range of the interaction, which we parameterize as $\xi = R_g/r$ with r the size of the colloid and R_g the radius of gyration of the polymer. Since the solvent mixture is a good solvent for PS, its radius of gyration varies somewhat with concentration; this also causes the osmotic pressure of the polymer solution to vary non-linearly with concentration. Therefore, we calibrate our polymer with static light scattering to experimentally determine the size of the polymer and the

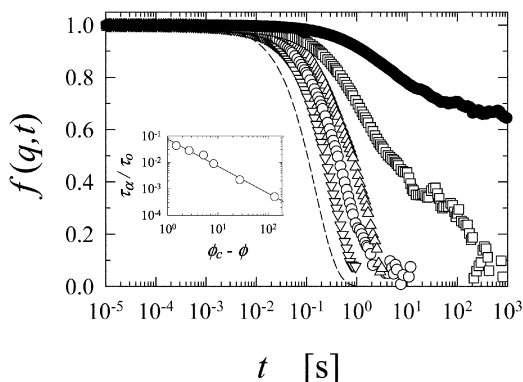


Fig. 2 Dynamic structure factor $f(q,t)$ at $qa = 0.85$ for a PMMA/PS system with $U/k_B T = 13.7$ and $\xi = 0.04$: [∇] $\phi = 0.024$; [\circ] $\phi = 0.039$; [\triangle] $\phi = 0.048$; [\square] $\phi = 0.066$; [\blacksquare] $\phi = 0.075$. The dotted line represents free diffusion of the particles. The inset shows the critical behavior of the decay time as ϕ_c is approached.

osmotic compressibility of the polymer solution as a function of concentration; we use these measured values in our calculation of the depletion interaction.¹⁷

A good measure of the approach to the phase boundary is provided by light scattering, which probes the structure and dynamics of the colloidal suspension. As the volume fraction approaches ϕ_c from below, low angle static light scattering from PMMA/PS systems exhibits a peak in the scattering intensity at small scattering wave vectors, q , reflecting the separation of clusters which must be nearly equally sized.^{14,18} The presence of these clusters is confirmed by confocal microscopy measurements.¹⁹ Their size is approximately consistent with a DLCA mechanism for aggregation; however, such a growth mechanism should lead to a gel and thus to an arrest of the cluster dynamics at any volume fraction. By contrast, we find that the speckles at the peak of the static scattering continue to fluctuate in time for samples below ϕ_c , indicating that the clusters move over length scales comparable to their size. To characterize these fluctuations, we measure the dynamic light scattering (DLS) at scattering wave vectors near the peak of the static scattering intensity. The temporal autocorrelation functions decay at all ϕ below ϕ_c ; however their decay times increase dramatically for small changes in ϕ , as shown in Fig. 2. The measured relaxation times diverge as $\tau_c \sim (\phi_c - \phi)^{-\alpha}$, where $\alpha \approx 1.1$; a similar divergence is observed for colloidal glasses, although there $\alpha \approx 2.5$.²⁰ Moreover, for any given volume fraction, the intermediate structure factors measured for all q can be scaled together,¹⁸ in the same fashion as those for colloidal glasses.²¹ This provides evidence for an analogy between the ergodic to non-ergodic transitions at low U and high ϕ , such as the colloidal glass transition, and the ergodic to non-ergodic transitions at high U and low ϕ .

We use light scattering to determine the phase behavior of the fluid to solid transition of the PMMA/PS system, and we identify the boundary between the fluid and solid gel states as a function of U and ϕ as well as ξ . The phase behavior of the gelation is strongly dependent on the range of the attraction, as shown in Fig. 3, where the circles represent data for systems with a longer range potential, $\xi \approx 0.16$ – 0.26 (the exact value depends on the polymer concentration), and the triangles represent data for a shorter range potential, $\xi \approx 0.04$; in both cases, the solid symbols represent the solid phase and open symbols represent the fluid phase. The dashed lines are guides to the eye that represent the phase boundary between the fluid and solid phases, as determined by the DLS. At higher volume fractions, $\phi > 0.10$, the fluid to solid transition occurs at significantly higher values of U for the shorter range potential than for the longer range potential; moreover, at the larger values of ϕ , the phase boundary is approximately independent of U . By contrast, as ϕ decreases below ~ 0.10 , the dependence on U becomes much stronger, with the phase boundary rising rapidly in U with little change in ϕ .

To more closely examine the behavior at these two limiting regimes of the phase boundary, we use rheological measurements. In the regime with high U , we measure the dependence of the

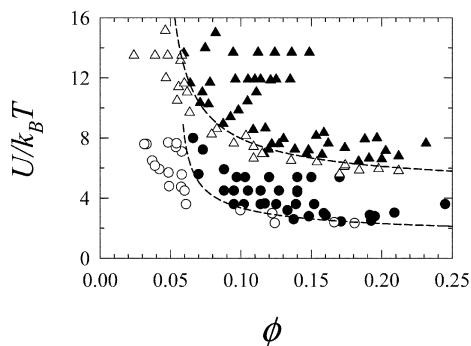


Fig. 3 Phase diagram for PMMA/PS systems of varying range of interaction potential, [O] $M_w = 2 \times 10^6$ g mol⁻¹, $\xi = 0.16$ –0.26 and [Δ] $M_w = 9.6 \times 10^4$ g mol⁻¹, $\xi = 0.035$ –0.045. Solid symbols indicate the solid cluster phase and open symbols the fluid cluster phase. The lines are guides to the eye, helping differentiate between the two phases.

viscoelastic response as a function of volume fraction at a fixed energy of attraction. The results exhibit a scaling behavior that is nearly identical to the one found for carbon black, and the master curve constructed from the PMMA/PS displays nearly the same shape as that obtained for the carbon black, as shown in Fig. 4 for $U/k_B T = 13.7$ and $U/k_B T = 11.9$ at low values of ξ and for $U/k_B T = 7.1$ and $U/k_B T = 5.8$ at large values of ξ . Moreover, the scaling factors a and b fall onto the same linear relationship as those for carbon black, provided a is normalized by η to account for the change in the background viscosity, as shown in Fig. 1(b). These results demonstrate the generality of this scaling behavior, which is identical for completely different colloid systems. These results also allow us to identify a value of ϕ_c with rheology. We again find a critical onset of G'_p ; however, the critical behavior is strongly dependent on the range of the potential as shown by the logarithmic plot of G'_p as a function of $\phi - \phi_c$ in Fig. 5. All the data are well described by $G'_p = G_0(\phi - \phi_c)^{v_\phi}$; however, the exponent varies significantly with the range of the interaction. For the long range potential, the exponent is $v_\phi \approx 2.1$, as shown by the dashed lines in Fig. 5; by contrast, for the short range potential, $v_\phi \approx 3.3$, as shown by the solid lines. In addition, the magnitude of G'_p is larger for the long range potential, even though U is lower.

A possible origin of the observed dependence of the exponent on the range of the interaction potential is rigidity percolation,^{22,23} which predicts a critical onset in the elastic modulus, $G'_p \sim (p - p_c)^\nu$, as bonds are randomly added to a medium, with probability, p . Both the critical

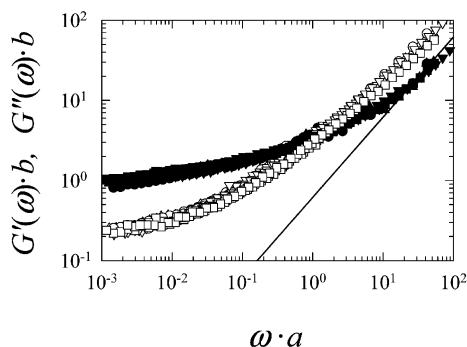


Fig. 4 Master curve for scaled moduli of the PMMA/PS systems, showing $G'(\omega)b$ [solid symbols] and $G''(\omega)b$ [open symbols], plotted as functions of scaled frequencies. Each symbol represents a scaled set of data obtained for different ϕ at fixed U and ξ : [Δ] $U/k_B T = 13.7$ and $\xi = 0.04$; [O] $U/k_B T = 11.9$ and $\xi = 0.04$; [∇] $U/k_B T = 7.1$ and $\xi = 0.17$; [\square] $U/k_B T = 5.4$ and $\xi = 0.18$. The solid line corresponds to the viscosity of a polymer-solution whose concentration is that of the free volume.

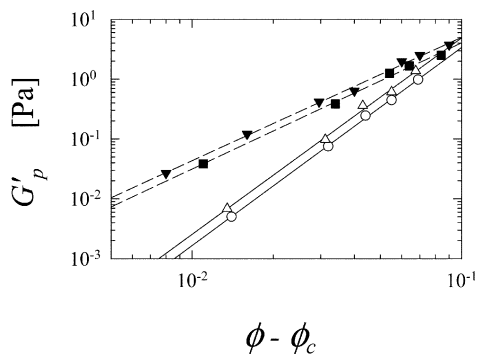


Fig. 5 Dependence of the plateau modulus and on the reduced volume fraction, $\phi - \phi_c$, for different ranges of the interaction potential. The short range potential has $\zeta \sim 0.04$, and data for $U/k_B T = 13.7$ [Δ] and $U/k_B T = 11.9$ [\circ]. The long range potential has $\zeta \sim 0.17$ – 0.18 , and data for $U/k_B T = 7.1$ [\blacktriangledown] and $U/k_B T = 5.4$ [\blacksquare]. Short-range potentials have critical exponents $\nu_\phi = 3.3 \pm 0.1$, shown by the solid line, while long-range potentials have $\nu_\phi = 2.10 \pm 0.05$, shown by the dashed line. The elastic modulus is larger for the long-range potential than for the short-range-potential, even though U is smaller.

value of the bond probability, p_c , and the critical exponent, ν , are sensitive to the nature of the bonds formed between the particles. If the interaction potential is centro-symmetric the bonds resist stretching but do not resist bending; then connectivity percolation is not sufficient for rigidity, and p_c for rigidity is greater than that for connectivity. Computer simulations suggest that the exponent describing the critical behavior in the bond stretching case is $\nu \approx 2.1$.²⁴ By contrast, if the individual bonds between particles can resist both stretching and bending, then p_c is the same for rigidity and connectivity; in this case, computer simulations suggest that $\nu \approx 3.75$.²⁵ The values of these exponents are in reasonable accord with the measured values, if we assume that the bonds formed by the shorter range potential can resist bending, while those formed by the longer range potential can not. However, an implicit assumption in this percolation picture is that the probability for bond formation, p , corresponds to the volume fraction, ϕ .

The difference in the exponents seems to imply differences in the nature of the basic interparticle bonds. The lower exponent, which occurs for the longer range potential, results from bonds between particles that do not resist bond bending, but instead only resist bond stretching. This is, in fact, what should be expected for a depletion interaction, where there should be no difference in the interaction energy for rotation of one particle with respect to its neighbor, provided the separation does not change. By contrast, the higher exponent which occurs for the shorter range potential, results from bonds which resist both bending and stretching. This implies a non-centro-symmetric interaction, which may arise because of the very short spatial extent of the interaction in this case; the range of this potential is sufficiently short that the average separation of the particles is only about 5 nm, which is comparable to the thickness of the stabilizing layer of poly-12 hydroxystearic acid. Thus, the interactions between the steric layers could conceivably make the potential non-centro-symmetric, thereby increasing the exponent. It is, therefore, tempting to attribute the difference in the exponents to a difference in the interparticle bonds, and their respective resistance, or lack thereof, to bending.

Some support for this microscopic picture of the nature of the interparticle bonds comes from confocal microscope studies of the dependence of the spring constant on particle separation.¹⁹ Structural studies of depletion gels suggest that any two particles are connected primarily by a single chain of particles; any additional loops are typically much longer than the primary chain. This allows us to measure the effective spring constant between two particles along a chain, and to determine the dependence of the spring constant on chain length. The spring constant is determined from the thermal fluctuations of the particles, which are assumed to have a Boltzmann distribution, with an energy controlled by the spring constant. The confocal microscopy measurements suggest that the spring constant for a long range potential scales with the number of particles in the chain, as expected for bonds that resist bond stretching only.²⁶ By contrast, the spring constant for a short

range potential also depends on the tortuosity of the chain, and scales with a higher power of the length of the chain, as expected for bonds that resist bending.²⁷ Thus, these results suggest that the local bonds do behave differently as the range of the interaction varies, and support the distinction in bonding mechanisms as the origin of the different exponents.

These experiments suggest that the phase boundary at high U results from rigidity percolation, and imply that there is a tenuous, fractal stress-bearing network, with a diverging correlation length at ϕ_c . However, the critical volume fraction depends on how it is measured; ϕ_c determined by rheology is higher than that determined by dynamic light scattering. The elasticity in the high U regime depends on a connected network of particles that can bear stress across the whole sample. By contrast, DLS measured near the peak in the structure factor does not actually probe the response of the network to a strain, but instead probes motion over length scales comparable to the average cluster size. It is conceivable that the clusters could become sufficiently crowded that they are not able to move enough to cause significant fluctuations of the speckles, even though they do not form a full stress-bearing network; this could result in a lower ϕ_c determined with DLS than with rheology. Thus, while light scattering determines an ergodic to non-ergodic transition, rheology determines the true rigidity and hence the fluid to solid transition.

The rheological behavior for lower U and higher ϕ is markedly different than that for the higher U . Because of the near independence of U_c on ϕ , it would be very difficult to measure a critical onset of elastic behavior by varying the volume fraction to determine ϕ_c . Thus, at lower U , we examine the rheological behavior by varying U at a fixed ϕ , for the longer range potential. We normalize the frequency with the ratio of the background viscosities, to account for the changes due to differences in the free-volume polymer concentration. For lower volume fractions, $\phi \sim 0.1$, the data exhibit behavior that is very similar to that observed when ϕ is varied at a fixed high U ; as shown in Fig. 6(a), there is a well defined low frequency plateau in the elastic modulus, and a cross over frequency where $G'(\omega)$ overtakes $G''(\omega)$. Both G'_p and the cross over frequency increase as U is increased, and the data can again be scaled onto a master curve similar to the one shown in Fig. 4. By contrast, at a higher volume fraction, $\phi \sim 0.2$, a completely different behavior is found; there is a clear relaxation at the lowest frequencies, and the hallmark of increasing the interaction energy is the decrease in the relaxation frequency, as shown in Fig. 6(b). These data suggest that instead of having a very rapid onset of a plateau modulus at the fluid to solid transition, there is instead a rapid decrease in the frequency of the final relaxation, while G'_p remains nonzero at ϕ_c .

The behavior at these higher values of ϕ is reminiscent of that observed for a colloidal glass, where there is no critical onset in the plateau modulus, but there is instead a critical divergence of the relaxation time.^{6,7} Thus, the high ϕ behavior of the fluid to solid transition seems to merge with that observed for a colloidal glass. Recent experiments have shown that there are two distinct classes of colloidal glass transition at the highest values of ϕ .²⁸ The first is a repulsive glass

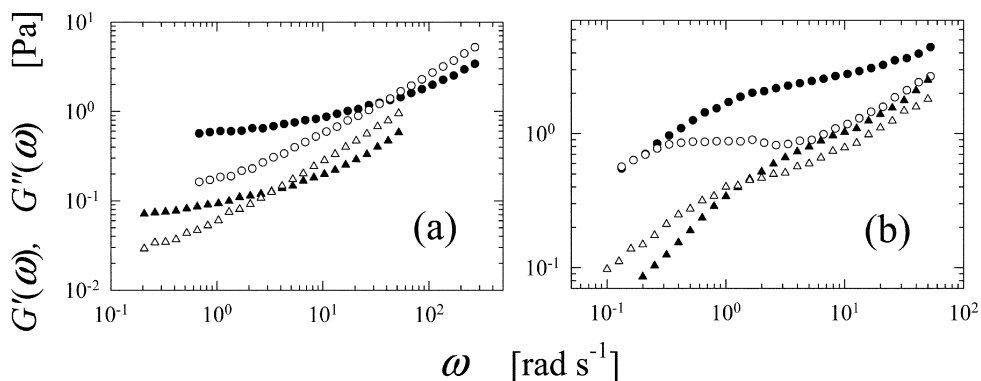


Fig. 6 Frequency dependence of $G'(\omega)$ [solid symbols] and $G''(\omega)$ [open symbols] for PMMA/PS systems with long-range potential. (a) $\phi \sim 0.1$ at $[\triangle] U/k_B T = 3.6$ and $[\circ] U/k_B T = 7.1$; (b) $\phi \sim 0.2$ at $[\triangle] U/k_B T = 2.0$ and $[\circ] U/k_B T = 3.0$. To account for changes in the free volume viscosity the frequency has been multiplied with η/η_{ref} with $\eta_{\text{ref}} = 8$ mPa s the background viscosity of the system at $U/k_B T = 2.0$.

transition, where $U = 0$, and where the glass transition is driven strictly by crowding of the particles. The second is an attractive glass transition, where U is slightly greater than zero, and the glass transition is driven by a combination of crowding and weakly sticking particles.^{28,29} The behavior we find with rheology at $\phi \sim 0.2$ suggests that the fluid to solid transition is similar across the low U regime, and is characterized by a glass-like transition.

While these data provide new insight into the behavior of the fluid to solid transition in this intermediate regime of ϕ and U , a complete understanding is still elusive. One proposed picture that may account for some of the features of this behavior was suggested in work presented at these discussions.³⁰ This proposal holds that there are two distinct types of fluid to solid transition. The first describes the behavior of the very local structure around any given particle, and determines the transition at the length scale of nearest neighbors. This transition does not reflect the behavior at larger length scales, which is essential in order to have a true solid. However, at high ϕ , the whole system is sufficiently crowded that it can undergo a fluid to solid transition, and this is the attractive glass transition.^{28,29,31,32} Support for this type of transition comes from our data for the rheology at high ϕ which exhibits glass-like behavior. At these high ϕ , the attractive glass transition seems to be reasonably well described by an extension of mode coupling theory to attractive interactions; this theory also predicts that the same gelation transition will extend to lower values of ϕ , with only a weak dependence on U .^{28,29,31,32} By contrast, at high U , the phase boundary rises rapidly in U with very little change in ϕ , and this can not be directly described by the same glass-like behavior, and is instead described by the second type of fluid to solid transition. Because of a hidden binodal or spinodal line in the attractive depletion interaction, the system tries to phase separate into colloid-rich and colloid-poor regions.^{33,34} Within any given colloid-rich region, the local volume fraction can become large enough to become locally solid, forming solid clusters. However, a solid network is only formed if the volume fraction of the clusters is large enough to span space, in which case they undergo a percolation transition. Our observation of a critical percolation-like behavior supports this type of fluid to solid transition, as does our observation of clusters below ϕ_c . We emphasize, however, that this whole picture is still very qualitative, with many details not determined; nevertheless, it does seem to successfully capture some of the overall behavior that we observe.

Jamming state diagram

Despite the differences in the details of the behavior, the fluid to solid transition has many more features in common, both as U and ϕ are varied over large ranges, and as completely different colloid systems are used. We illustrate this generality in Fig. 7(a), where we plot G'_p as a function of ϕ for colloidal gels formed from carbon black and from PMMA/PS. For comparison, we choose the data for the short range interaction, $\xi \approx 0.04$, where the bonds resist both bending and stretching. We focus on the behavior at high U , where the viscoelastic data exhibit scaling behavior, with a critical onset of G'_p . In all cases, the plateau modulus grows in a critical fashion, with $G'_p = G_0(\phi - \phi_c)^{\nu_\phi}$, where the exponent, ν_ϕ , varies between 3.3 and 4.1. In Fig. 7(a) we also include rheological data obtained from a colloidal gel formed from buoyancy-matched polystyrene latex spheres in water,⁴ where irreversible aggregation is induced through the addition of salt, which leads to a very strong attractive interaction between particles.^{1,3,4,56} The plateau modulus again increases in a critical fashion, but in this case, the critical volume fraction is $\phi_c = 0$. The coefficient, G_0 , that describes the magnitude of the plateau modulus for each set of gels, is a strong function of the magnitude of the interaction, increasing sharply with increasing U ; this is shown clearly by the increasing values of G'_p as U increases from the PMMA/PS to the carbon black, and then to the irreversibly aggregated PS. Thus, both the critical volume fraction and the magnitude of the elasticity depend sensitively on the strength of the attractive interaction between particles; as U increases, ϕ_c decreases and G'_p increases.

To determine the behavior of these samples along the third axis of the jamming state diagram, we also measure the yield stress, σ_y , of our samples. We do this by making oscillatory measurements of $G'(\omega)$ as a function of the maximum applied strain, γ , and identify the yield strain, γ_y , as the value of the strain where the storage modulus first becomes dependent on γ ; the yield stress is then calculated using $\sigma_y = G'_p \gamma_y$. The overall dependence of σ_y on U and ϕ is similar to that observed for G'_p , as shown in Fig. 7(b). The dependence of the yield-stress in volume fractions is again well

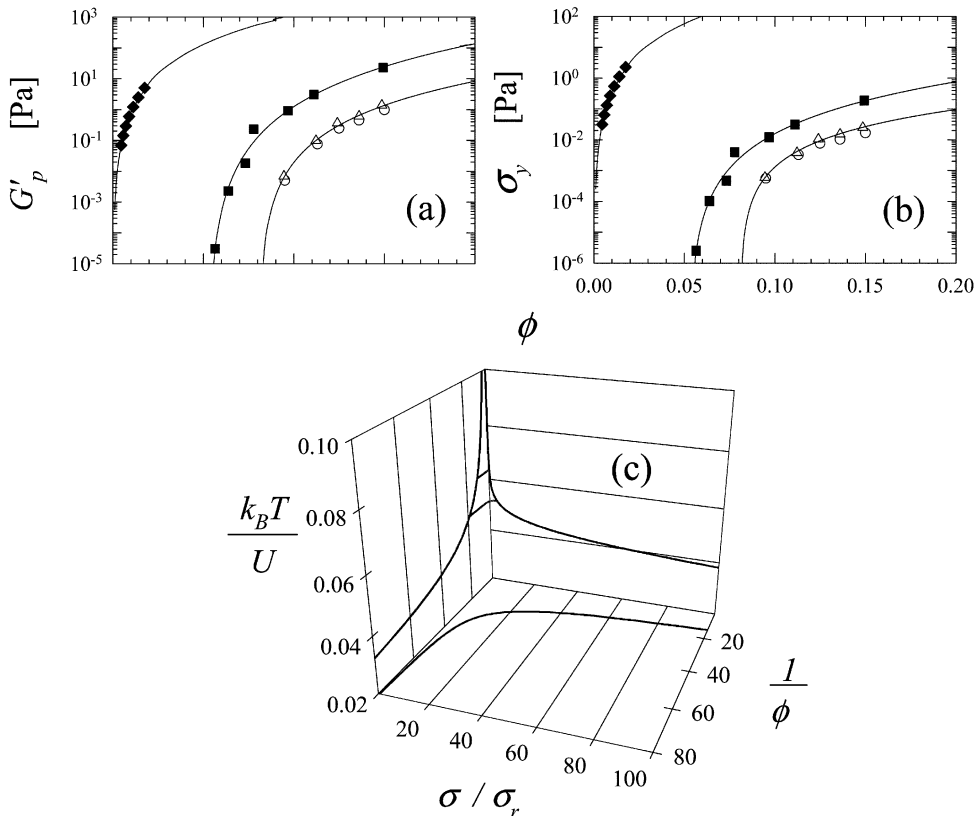


Fig. 7 Solid-like properties and jamming state diagram for systems with short-range potential: [◆] polystyrene particles gels; [■] carbon black; [△] PMMA/PS with $U/k_B T = 13.7$ and $\xi = 0.04$; [○] $U/k_B T = 11.9$ and $\xi = 0.04$. (a) Critical onset and increase of the elastic modulus with ϕ . (b) Critical onset and increase of the yield stress with ϕ . To account for changes in the particle size, both, G'_p and σ_y have been multiplied with r/r_{ref} with $r_{\text{ref}} = 136$ nm, the size of the PMMA particles. (c) Jamming state diagram for $\phi < 0.3$ and $U/k_B T > 10$, where σ has been normalized by $\sigma_r = k_B T/r^3$, to make it dimensionless.

described by a critical-like behavior, with $\sigma_y = \sigma_0(\phi - \phi_c)^{\mu_\phi}$, where the exponent, μ_ϕ , varies between 2.2 and 3.4. Again, both the critical volume fraction and the magnitude of the yield stress depend on U ; as U increases, ϕ_c decreases and σ_y increases.

These yield stress data provide the basis for the jamming state diagram, which provides an excellent means to collate the behavior.⁸ The yield stress represents the boundary between the fluid and solid states, and, in Fig. 7(c), we show a schematic jamming state diagram based on these data and the critical-like dependence of σ_y on ϕ obtained for the PPMA/PS, carbon-black and the polystyrene gels. If the yield stress is exceeded the colloidal network is destroyed, and the sample is fluidized. The boundary set by the yield stress shifts systematically to larger values of σ_y as either U or ϕ is increased. The solid-like or jammed state of attractive colloidal particles exists for sufficiently low values of ϕ^{-1} , for sufficiently low values of U^{-1} , and for sufficiently low values of σ . An increase along any one of these axes will fluidize the solid like state if the jamming state boundary is crossed; thus a lower interaction energy, a lower volume fraction or a higher external stress will each lead to a solid to fluid transition. By using the axes chosen, a solid state exists in the inner octant of the jamming state diagram. We emphasize, however, that the jamming state diagram shown in Fig. 2(c) represents a portion of the diagram, restricted to $\phi < 0.3$ and $U > 10k_B T$; the behavior at higher values of ϕ and lower values of U , which would appear near the origin of the ϕ^{-1} axis and at large values of U^{-1} , are not a simple extrapolation of the data shown in Fig. 7(c). In particular, the critical onset of the elasticity and of the yield stress is observed only at sufficiently

high U . The behavior at lower U does not exhibit a critical onset; instead, G'_p and σ_y are non-zero at ϕ_c or U_c , reminiscent of a colloidal glass.³⁵ Consistent with this the rheological response at volume fractions slightly below the transition exhibits an intermediate regime in frequency where $G'(\omega)$ dominates over $G''(\omega)$, followed by a lower frequency terminal relaxation regime, like this observed in colloidal glasses.^{6,7} The transition can be identified by the diverging relaxation time, rather than from the onset of elasticity and the scaling behavior.

The primary utility of the jamming description of the fluid to solid transition for attractive colloidal particles is that it unifies the disparate behavior of many different systems, describing them under a single rubric. The key unifying feature of the jamming transition is the sudden arrest of the internal dynamics, which leads to solid-like properties. This arrest is driven by crowding of the system; however the basic object that becomes crowded varies. For very low ϕ , and very high U , it is the fractal clusters that become crowded and jam to form a solid; a gel is formed when the volume fraction of fractal clusters becomes unity. Similarly, for the intermediate volume fractions, it is again the clusters that jam to form the solid phase. By contrast, at the larger volume fractions, it is the individual particles that become crowded and jam to form the solid phase. Despite these differences, the behavior is remarkably similar in each of the three cases when the transition is approached from the fluid-side; here we find an ergodic to non-ergodic transition, which exhibits remarkable similarities over wide ranges of U .

Conclusions

It is useful to briefly summarize those features of the jamming phase behavior that are well understood and those which are as yet unclear. In the absence of any applied stress, the phase behavior is well understood in the two limiting regimes: At high ϕ and very low U , the fluid to solid transition is a colloidal glass transition, which can be either repulsive or attractive depending on the exact value of U . In the jamming state diagram, this occurs when $k_B T/U$ becomes very large, but ϕ^{-1} becomes very small. At very low ϕ and very high U , the fluid to solid transition results from irreversible aggregation which forms fractal clusters which gel. In the jamming state diagram, this occurs when $k_B T/U$ becomes very small, but ϕ^{-1} becomes very large. In the intermediate regime, the details are not as well understood, although the possible combination of a local attractive glass transition with an incipient phase separation may offer some potential explanation, albeit incomplete.³⁰

There are some features of this intermediate regime that appear to be universal. Over the whole regime, there appears to be a ergodic to non-ergodic transition, as probed by DLS, whose character is similar to that of the colloidal glass transition. Similar glass-like behavior is seen in the rheology for the low U portion of this regime. By contrast, at high U , the behavior is critical, with a sudden onset of the elasticity. This behavior appears to be universal in itself, as all colloidal systems investigated seem to have the same scaling behavior.

These features seem to be in accord with the jamming concept. In all cases, the fluid to solid transition is caused by crowding of the system, which leads to kinetic arrest and the formation of stress bearing paths. These paths are more transient in nature for the region characterized by the glass transition, and thus a much higher volume fraction is required for the fluid to solid transition. By contrast, they are much more permanent in nature at low volume fractions, requiring a much higher value of U . In this case the stress bearing paths are well defined, and are much sparser, and they span space at the fluid to solid transition. The nature of these stress bearing paths also determines the nature of the yield stress for the material, and hence the third phase boundary in the jamming state diagram. In fact, this is one of the most useful features of the description of the fluid to solid transition with the jamming state diagram—it offers a direct description of the materials properties because it focuses on the stress bearing paths of the solid. Thus, the greater the ability of the solid to bear stress, the larger is its modulus, and the larger will be its yield stress. This is directly captured by the jamming state diagram.

The description of the fluid to solid transition by means of the jamming state diagram provides a description that captures many of the universal features of the fluid to solid transition. However, there are many other aspects of the transition that are not completely described within this picture. One of the most important is the time evolution of the transition. The nature of the solid state

depends sensitively on the history of the evolution of the fluid to the solid. Such a gelation process is in part controlled by the diffusion of the particles and clusters, which allows them to form the network; thus the detailed structure of the solid network can vary somewhat as the gelation occurs. This sensitivity is even stronger if a stress is applied while the sample is evolving from a fluid to a solid. Similarly, the behavior of the sample will also continue to evolve even after the solid is formed; such aging is ubiquitous in samples of this sort. Nevertheless, the jamming state diagram provides a valuable means of summarizing the behavior.

Acknowledgements

We gratefully acknowledge support for this work from NASA (NAG3-2284) and the NSF (DMR-9971432).

References

- 1 M. Carpineti and M. Giglio, *Phys. Rev. Lett.*, 1992, **68**, 3327.
- 2 J. Bibette, T. G. Mason, H. Gang and D. A. Weitz, *Phys. Rev. Lett.*, 1992, **69**, 981.
- 3 A. H. Krall and D. A. Weitz, *Phys. Rev. Lett.*, 1998, **82**, 1064.
- 4 T. Gisler, R. C. Ball and D. A. Weitz, *Phys. Rev. Lett.*, 1999, **82**, 1064.
- 5 P. N. Pusey and W. van Meegen, *Phys. Rev. Lett.*, 1987, **59**, 2083.
- 6 T. Shikata and D. S. Pearson, *J. Rheol.*, 1994, **38**, 601.
- 7 T. G. Mason and D. A. Weitz, *Phys. Rev. Lett.*, 1995, **74**, 2770.
- 8 V. Trappe, V. Prasad, L. Cipelletti, P. N. Segre and D. A. Weitz, *Nature*, 2001, **411**, 772.
- 9 A. J. Liu and S. R. Nagel, *Nature*, 1998, **396**, 21.
- 10 V. Trappe and D. A. Weitz, *Phys. Rev. Lett.*, 2000, **85**, 449.
- 11 T. G. Mason, J. Bibette and D. A. Weitz, *Phys. Rev. Lett.*, 1995, **75**, 2051.
- 12 D. M. A. Buzza, C.-Y. D. Lu and M. E. Cates, *J. Phys. II*, 1995, **5**, 37.
- 13 P. Sollich, F. Lequeux, P. Hebraud and M. E. Cates, *Phys. Rev. Lett.*, 1997, **78**, 2020.
- 14 P. N. Pusey, A. D. Pirie and W. C. K. Poon, *Physica A*, 1993, **201**, 322.
- 15 P. N. Pusey and W. v. Meegen, *Nature*, 1986, **320**, 340.
- 16 H. N. W. Lekkerkerker, W. C. K. Poon, P. N. Pusey, A. Stroobants and P. B. Warren, *Europhys. Lett.*, 1992, **20**, 559.
- 17 V. Prasad, V. Trappe, A. D. Dinsmore and D. A. Weitz, 2002, unpublished data.
- 18 P. N. Segre, V. Prasad, A. B. Schofield and D. A. Weitz, *Phys. Rev. Lett.*, 2001, **86**, 6042.
- 19 A. D. Dinsmore and D. A. Weitz, *J. Phys.: Condens. Matter*, 2002, **14**, 7581.
- 20 W. van Meegen and S. M. Underwood, *Phys. Rev. E*, 1994, **49**, 4206.
- 21 P. N. Segre and P. N. Pusey, *Phys. Rev. Lett.*, 1996, **77**, 771.
- 22 S. Feng, P. N. Sen, B. I. Halperin and C. J. Lobb, *Phys. Rev. B*, 1984, **30**, 5386.
- 23 M. Sahimi and S. Arbabi, *Phys. Rev. B*, 1988, **38**, 7173.
- 24 S. Arbabi and M. Sahimi, *Phys. Rev. B*, 1993, **47**, 695.
- 25 M. Sahimi and S. Arbabi, *Phys. Rev. B*, 1993, **47**, 703.
- 26 A. A. Potanin and W. B. Russel, *Phys. Rev. E*, 1996, **53**, 3702.
- 27 Y. Kantor and I. Webman, *Phys. Rev. Lett.*, 1985, **52**, 1891.
- 28 K. N. Pham, A. M. Puentes, J. Bergenholtz, S. U. Egelhaaf, A. Moussaid, P. N. Pusey, A. B. Schofield, M. E. Cates, M. Fuchs and W. C. K. Poon, *Science*, 2002, **296**, 104.
- 29 T. Eckert and E. Bartsch, *Phys. Rev. Lett.*, 2002, **89**, 125701.
- 30 K. Kroy, M. Fuchs, M. E. Cates, P. N. Pusey and W. C. K. Poon, 2002, private communication.
- 31 J. Bergenholtz and M. Fuchs, *Phys. Rev. E*, 1999, **59**, 5706.
- 32 J. Bergenholtz, M. Fuchs and T. Voigtmann, *J. Phys.: Condens. Matter*, 2000, **12**, 6575.
- 33 S. M. Ilett, A. Orrock, W. C. K. Poon and P. N. Pusey, *Phys. Rev. E*, 1995, **51**, 1344.
- 34 W. C. K. Poon, F. Renth, R. M. L. Evans, D. J. Fairhurst, M. E. Cates and P. N. Pusey, *Phys. Rev. Lett.*, 1999, **83**, 1239.
- 35 M. Fuchs and M. E. Cates, *Faraday Discuss.*, 2003, **123** (DOI: 10.1039/b205629a).
- 36 L. Cipelletti, S. Manley, R. C. Ball and D. A. Weitz, *Phys. Rev. Lett.*, 2000, **84**, 2275.